A chaperonin containing T-complex polypeptide-1 facilitates the formation of the PbWoxT1 -PbPTB3 ribonucleoprotein complex for long-distance RNA trafficking in Pyrus betulaefolia

Shengnan Wang, Xuwei Duan, Shengyuan Wang, Li Hao, Yi Zhang, Chaoran Xu, Yunfei Yu, Ling Xiang, Feng Jiang, Manfred Heinlein, et al.

Li Tianzhong (Orcid ID: 0000-0003-4076-231X)

Zhang Wenna (Orcid ID: 0000-0003-4094-9766)

A chaperonin containing T-complex polypeptide-1 facilitates the formation of the *PbWoxT1*-PbPTB3 ribonucleoprotein complex for long-distance RNA trafficking in *Pyrus betulaefolia*

Authors: Shengnan Wang[1], Xuwei Duan[1], Shengyuan Wang[1], Li Hao[1], Yi Zhang[1], Chaoran Xu[1], Yunfei Yu[1], Ling Xiang[1], Feng Jiang[1], Manfred Heinlein[2], Tianzhong Li[1]*, Wenna Zhang[1] *

Author Affiliations:
1 College of Horticulture, China Agricultural University, 100193, Beijing, China
2 Institut de biologie moléculaire des plantes, CNRS, Université de Strasbourg, 67084, Strasbourg, France

Corresponding Authors Email Address:
litianzhong1535@163.com
zhangwenna@cau.edu.cn

Received: *9 November 2022*
Accepted: *29 January 2023*

Key words: CCT, assembly, RNP complex, long-distance trafficking, *Pyrus betulaefolia*.

ORCID:
Tianzhong Li, http://orcid.org/0000-0003-4076-231X
Wenna Zhang, http://orcid.org/0000-0003-4094-9766
Manfred Heinlein, http:// orcid.org/0000-0001-7322-1654

Summary

- Numerous plant endogenous mRNAs move via phloem and thus affect the growth and development of long-distant organs. mRNAs are transported with RNA-binding proteins forming a ribonucleoprotein complex. However, it remains elusive how such RNP complex assembles and facilitates mRNA trafficking.
- Protease digestion and RNA immunoprecipitation were used to investigate the RNP assembly function of the complete Chaperonin Containing T -complex Polypeptide-1. *In situ* hybridization, hairy root transformation, microprojectile bombardment and grafting experiments demonstrate the role of CCT complex in the transport of a *PbWoxT1*-PbPTB3 RNP complex in *Pyrus betulaefolia*.
- PbCCT5 silenced caused defective movement of GFP-PbPTB3 and *GFP-PbWoxT1* from hairy roots to new leaves via the phloem. PbCCT5 is shown to interact with PbPTB3. PbCCT complex enhanced PbPTB3 stabilization and permitted assembly of *PbWoxT1* and PbPTB3 into an RNP complex. Furthermore, silencing of individual *CCT* subunits inhibited the intercellular movement of GFP-PbPTB3 and long-distance trafficking of *PbWoxT1* and PbPTB3 in grafted plants.
- Taken together, the CCT complex assembles PbPTB3 and *PbWoxT1* into an RNP complex in the phloem in order to facilitate the long-distance trafficking of *PbWoxT1* in *P. betulaefolia*. This study therefore provides important insights into the mechanism of RNP complex formation and transport.

Introduction

The phloem sieve tube system (STS) of plants functions as a major conduit for the long-distance transport of nutrients (sugars and amino acids) and signaling molecules (e.g., hormones, RNAs, proteins) from mature, 'source' tissues to developing 'sink' tissues (Lucas et al., 2013; Ham and Lucas, 2016). Mobile RNA molecules, including mRNAs and non-coding RNAs traffic from companion cells (CC) into sieve elements (SE) through plasmodesmata (PD) to achieve long-distance transport (Haywood et al., 2002; Lucas et al., 2013; Ham and Lucas, 2016; Kehr et al., 2021). Grafting scions of one genotype to rootstocks of another genotype is a widely used procedure in fruit trees to enable the exchange of nutrients and signaling factors between two genotypes upon re-construction of the vasculature system (Tsutsui and Notaguchi, 2017; Huang et al., 2018). Several studies employing grafting demonstrated that numerous mRNA

molecules in *Arabidopsis thaliana* (Lu et al., 2012; Notaguchi et al., 2012), potato (*Solanum tuberosum*) (Banerjee et al., 2006), tomato (*Solanum lycopersicum*) (Kim et al., 2001), pumpkin (*Cucurbita maxima*) (Ruiz-Medrano et al., 1999) and pear (*Pyrus betulaefolia*) (Duan et al., 2016; Hao et al., 2020) are mobile within phloem and can move over long-distances between rootstock and scion across a graft union. Several mobile mRNAs species were shown to participate in the long-distance regulation of biological functions, such as *CmNACP* (Ruiz-Medrano et al., 1999), *CmGAIP* (Haywood et al., 2005), *StBEL5* (Banerjee et al., 2006), and *PFP-Let6* (Kim et al., 2001) in apical meristem development, hormone metabolism, tuber growth and leaf morphology, respectively. In nature, RNA molecules need to interact with proteins to form ribonucleoprotein (RNP) complexes and thus to enhance RNA stability and transport in the phloem translocation stream (Ham and Lucas, 2016). The best characterized phloem RNP complexes to date involve polypyrimidine tract binding (PTB) proteins, which bind mRNAs harboring a CUCU domain. For example, the *Cucurbita maxima* RNA-binding protein 50 (CmRBP50) was shown to form a graft-transmissible RNA-protein complex detected in the phloem sap (Ham et al., 2009). Furthermore, other components of the complex, such as CmNACP1, combined with CmRBP50 to jointly bind RNA, thus enhanced the stability of the complex (Li et al., 2011). However, the pathway through which mRNAs and RNA binding proteins (RBPs) form phloem-mobile RNP complexes is unclear.

The formation of RNP complexes by RBPs generally requires the correct folding of the newly synthesized polypeptide chains into native configurations that can bind the RNA molecules, and involves protein phosphorylation, RNA-methylation and other intricate processes (Li et al., 2011; Roh et al., 2016; Paul et al., 2019). In many or most cases, these processes require chaperonins to stabilize folding intermediates, maintain protein homeostasis and folded protein structures, and to mediate in transmembrane and intercellular transport (Horwich et al., 2007). CCT/TRiC (Chaperonin containing T-complex polypeptide-1/ T-complex polypeptide-1 ring complex) is a eukaryotic cytosolic group Ⅱ chaperonin known in yeast and mammals. This chaperonin consists of eight subunits (CCT1-CCT8) that form a large (1000 kDa) hetero-

oligomeric complex, in which the subunits are arranged in a specific order and form double rings stacked back-to-back (Frydman, 2001; Horwich et al., 2007; Leitner et al., 2012). The CCT complex helps proteins to fold into their active state by encapsulating unfolded substrate proteins within the central cavities of the complex in an ATP-dependent manner (Cong et al., 2012). Different substrates were shown to be bound by different CCT subunits, which is mainly due to highly divergent apical domains of the eight CCT subunits (Spiess et al., 2006; Horwich et al., 2007). Initially known substrates of CCT were actin, α-tubulin and β-tubulin, which are abundant in the cytoplasm (Yaffe et al., 1992; Yijie et al., 1992). However, CCT may have many other substrates, as indicated by more recent studies. For example, CCT was shown to participate in the folding of tumor suppressors (VHL and p53) (Spiess et al., 2006) and cell cycle regulators (CDC20 and CDH1) (Camasses et al., 2003). Moreover, both CCT5 and the whole CCT complex assist in the folding of tubulins in maize (Himmelspach et al., 1997), oats (Moser et al., 2000) and *Arabidopsis* (Ahn et al., 2019). In an Arabidopsis trichome rescue assay, Arabidopsis *CCT8* and an RNA exosome protein *AtRRP44A* were shown to facilitate the cell-to-cell trafficking of KNOTTED mRNA and protein via plasmodesmata (Xu et al., 2011; Kitagawa et al., 2022). Moreover, the efficiency of the movement protein-dependent spread of *Oilseed rape mosaic virus* was reduced in a *cct8* mutant suggesting a role of CCT8 in intercellular transport of viral movement proteins (Fichtenbauer et al., 2012). However, the range of protein substrates of the CCT complex, the mechanism by which and how the CCT complex supports the assembly of proteins together with viral or host RNA molecules into RNPs, and whether the biological functions of CCT in the specific protein substrates is conserved between plant species remain to be further explored.

In a previous study, we found that *P. betulaefolia* PbPTB3 binds to *PbWoxT1* (WUSCHEL-RELATED HOMEOBOX Transport 1) mRNA and facilitates the movement of this mRNA across graft unions, thus indicating that RNP formation is a critical step for the long-distance transport of this mRNA (Duan et al., 2016). In searching for co-factors assisting in the movement of the PbPTB3-associated RNP complex, we here identified PbCCT5, one of the eight subunits of the PbCCT complex

in *P. betulaefolia*. We demonstrate that the complete PbCCT complex is required for the formation of the *PbWoxT1*-PbPTB3 RNP complex and its long-distance trafficking in *P. betulaefolia*. Silencing of CCT subunits compromised the movement of PbPTB3 and *PbWoxT1* by preventing assembly of RNP complexes. Our findings identify PbPTB3, the core of the *PbWoxT1*-PbPTB3 RNP complex, as a novel substrate for CCT and reveals the role of the CCT complex in mediating the long-distance trafficking of the RNP complex in *P. betulaefolia*.

Materials and Methods

Plant material and growth conditions

P.betulaefolia tree (*Pyrus betulaefolia* Bunge) were grown at the experimental farm of China Agricultural University, Beijing, China. Pear seeds were cultured in soil under conditions of 24℃ with a 16 h:8 h light:dark photoperiod under 100–500 μmol $m^{-2}s^{-1}$ light intensity provided by cool-white fluorescent tubes and a relative humidity of >95%. Pear 'Zhongai no.1' [(*Pyrus ussuriensis* × *communis*) × spp.] cambium calluses were tissue cultured in Murashige and Skoog (MS) medium with 2.5 mg/ml 2,4-dichlorophenoxyacetic acid (2,4-D) and 1 mg/ml 6-benzylaminopurine (Murashige & Skoog + 2.5 mg/L 6-benzylaminopurine (6-BA) +2 mg/L 2,4-dichlorophenoxyacetic acid (2,4-D) + 0.5 mg/L 3-Indoleacetic acid (IAA)) at 24℃ under 24-h darkness and a relative humidity of 80%. *N.benthamiana* (*Nicotiana benthamiana*) and *N.tabacum* (*Nicotiana tabacum* var. Wisconsin 38) plants were tissue-cultured in MS medium without hormones at 24℃ with a 16 h:8 h light:dark photoperiod under a 100–500 μmol $m^{-2}s^{-1}$ light intensity provided by cool-white fluorescent tubes and a relative humidity of 80%.

In situ hybridization

The stems of 1 year old *P.betulaefolia* tree (*Pyrus betulaefolia* Bunge) were fixed in 3.7 % FAA (3.7% formaldehyde, 5% acetic acid, and 50% ethanol) at 4℃ overnight with vacuum infiltration. Embedding, hybridization, and detection were carried out according to methods described previously (Nie et al., 2021). The embedded samples were sectioned into 8 μm slices by both transverse and longitudinal sections with

paraffin slicer (Leica RM2125 RTS). The 479 bp fragment recogning 643-1122 bp of *PbCCT5* was used for sense and antisense probes, which were amplified with specific primers using the DIG RNA Labeling Kit (SP6/T7) (Roche 11175025910). Anti-digoxigenin, conjugated to alkaline phosphatase (AP), was used to detect digoxigenin-labeled RNAs. The *PbSUC2* probe was used as the marker. Images were obtained with an Olympus BX53 and CX23 microscope (Olympus, Japan). The primer sequences used are listed in Table S1.

Immunogold transmission electron microscopy

Immunoelectron microscopy was performed as described previously (Liu et al., 2019). The phloem of *P. betulaefolia* stem (Fig. S1), which was easily specific dissected as previously established method (Duan et al., 2016), were fixed in 4% (v/v) paraformaldehyde in 0.1 M PBS (pH 7.2) and embedded in LR White medium (Electron Microscope Science Inc, EMS). Ultrathin sections (85 nm) were cut with Ultracut (Reichert-Jung Ultracut E Ultramicrotome, Leica, Germany) with a diamond knife and mounted onto nickel grids. The grids were blocked by 5% non-fat milk in 1× TBST for 1 h and subsequently incubated with anti-PbCCT5 (Baitailong Bio) antibody overnight at 4℃. The grids were washed five times with 1×TBST and incubated with 15-nm gold-conjugated goat anti-rabbit antibody (Abcam) at 1:20 (v/v) dilution in a blocking solution for 40 min. The grids were then washed five times with 1× TBST and twice with sterile distilled water. Photographs were taken with a transmission electron microscope (JEM-1230).

Hairy root stable transformation and CFDA assay

Hairy root transformation was performed as described previously (Meng et al., 2019; Cao et al., 2022) with minor modification. The *P. betulaefolia* seeds were stratified at 4℃ for 3 weeks and then planted in soil for *Agrobacterium*-infiltration 1 week later using the following the stable transformation procedure. Cultures of *Agrobacterium rhizogenes* (*Rhizobium rhizogenes*) strain K599 harboring pCAMBIA1305.1 derived vectors *pSUC2::GFP-PbPTB3*, *pSUC2::GFP-PbWoxT1*, *pSUC2::GFP-PbCCT5* or pFGC5941-derived vector *p35S:hpPbCCT5* (Methods S1) were grown overnight in 5 ml YEP liquid medium with 50 mg/L rifampicin and 50 mg/L kanamycin with shaking at 160 g at 28℃. At an OD_{600} value of 1.0, the cultures were injected into plant stems 1 cm above the soil (Fig. S2). The stems were then broken with a needle and laid flat

on the soil. The plants were then cultured at >95% humidity for about 2 weeks until hairy roots grew at the infection site on the stem. The stable transformed hairy roots were planted in the soil and the leaves and shoot apex were removed from the stems leaving the initiation of the first true leaf above the cotyledons. The plants were allowed to grow until the first true leas developed in the initiation about 2 weeks later. Root, hypocotyl, leaves before transformation and hairy root, hypocotyl, new leaf after transformation were collected 28 d after the original agroinfiltration to perform RT-PCR and western blot analysis. In addition, hairy roots were soaked in 1 mg/ml 5-Carboxyfluorescein diacetate (CFDA) (dissolved in DMSO) for 2 h to investigate symplastic CFDA trafficking from the roots into the new leaves. The hairy roots and the new leaves were observed with a confocal laser fluorescence microscope (Nikon A1).

Purification of the PbCCT complex from pear leaves

Total protein of *P. betulaefolia* leaves was extracted using the Plant Total Protein Extraction Kit (HuaXingBoChuang Bio) to purify the PbCCT complex as previously described with minor modifications (Ferreyra and Frydman, 2000). The total protein was applied to an anion-exchange column of DE52 cellulose and then subjected to ammonium sulfate fractionation, gel-filtration chromatography on a Sephacryl S-300 column, ion-exchange chromatography on a high-resolution Mono Q column, affinity chromatography on a HiTrap heparin column and, finally, high-resolution Superose 6 gel-filtration chromatography. The purity of the PbCCT complexes, determined by 10% SDS-PAGE (Fig. S3) and mass spectrometry analysis (Table S2), was suitable for use in the proteinase K (PK) digestion assay and REMSA (Methods S1).

PK digestion assay

PK digestion assay was performed as described previously (Bai et al., 2015; Roh et al., 2016) in buffer E (25 mM HEPES pH7.5, 100 mM KOAC, 10 mM Mg $(OAC)_2$, 2 mM DL-dithiothreitol (DTT), 200 mM NaCl, 10% [v/v] glycerol and 1mM ATP), containing a 5:1 molar ratio of substrate to chaperonin with the final concentration 2.5 μg/μl:0.5 μg/μl. For each reaction system, the total amount of PbCCT subunits was consistent. The binding mixture, consisting of PbCCT1 through PbCCT8 combined with PbPTB3, was incubated at 30 ℃ for 30 min, after which 0.1 mg/ml protease was added and the mixture was further incubated for 8 min at 25℃. PK digestion was stopped with 1 mM

phenylmethylsulfonyl fluoride (PMSF). Reactions were analyzed on a 10% SDS-PAGE gel followed by immunoblotting.

RNA-protein pull-down assay

PbWoxT1 mRNA was obtained by in vitro transcription using the T7 RiboMAXTM Express Large Scale RNA Production System (Promega). The mRNA was labeled with desthiobiotinylated cytidine bisphosphate (pCpdesthiobiotin) using the Pierce™ RNA 3' End Desthiobiotinylation Kit (Thermo Fisher Scientific, Rockford, IL, USA). GST tagged PbPTB3 proteins were expressed in *E.coli* BL21 (DE3) and purified to GST-BindTM Resin (Novagen, San Diego, CA, USA) following the supplier's protocol. RNA-protein pull-down was performed using the PierceTM Magnetic RNA-Protein Pull-Down Kit (Thermo Fisher Scientific). Briefly, *PbWoxT1* mRNA-bound beads were equilibrated in Protein-RNA Binding Buffer before 40 μg PbPTB3 protein was added. Following incubation for 60 min at 4°C with rotation, the beads were then washed with a wash buffer, vortexed and separated on a magnetic stand. Samples were eluted from the beads using nondenaturing Biotin Elution Buffer and assessed by Western blot analysis and RT-PCR analysis. For denaturation analysis, 6 M guanidine-HCl was added to the above reaction system together with *PbWoxT1* and PbPTB3. To assess the ability of the PbCCT complex to refold PbPTB3 after denaturation, 6 M guanidine-HCl was added to the above reaction system followed by rapidly diluted 100-fold into ice-cold refolding buffer A (25 mM HEPES at pH 7.5, 100 mM KOAc, 10 mM $Mg(OAc)_2$, 2 mM DTT, 10 mM creatine phosphate, 200 mM NaCl, 10% glycerol) with or without PbCCT complex, using a 5:1 molar ratio of PbPTB3 substrate to PbCCT. The reaction mixture was incubated at 30 ℃ for 1 h (Roh et al., 2016), followed by washing beads and next steps.

Callus transformation of *Pyrus*

The phloem of pear 'Zhongai 1' [(*Pyrus ussuriensis* × *communis*) × spp.] was disinfected with 75% alcohol 1 min and 2% sodium hypochlorite 15 min, following cultured in dark on culture medium (Murashige & Skoog + 2.5 mg/L 6-benzylaminopurine (6-BA) +2 mg/L 2,4-dichlorophenoxyacetic acid (2,4-D) + 0.5 mg/L 3-Indoleacetic acid (IAA)) until callus grew. Callus proliferation culture was used for subsequent transgenic. The vector of *p35S:hpPbCCT5* on pFGC5941 was transformed into *Agrobacterium tumefaciens* GV3101 and cultured for 2-3 days on YEP medium (10 g/L Yeast extract, 10 g/L Tryptone, 5 g/L NaCl, 10 g/L agar powder)

containing kanamycin and rifampin. Each positively transformed colony was cultured in YEP liquid medium overnight, harvested at 5,300g for 5 min at room temperature and resuspended in inducing buffer (10 mM $MgCl_2$, 0.2 mM acetosyringone and 10 mM 2-(4-morpholino) ethanesulfonic acid (MES), pH 5.6) to a concentration of OD_{600} = 1.0. After being resuspension with MS pH 5.2, the callus was placed in it and shaken for 3 min, then sucked out the excess solution on sterilized filter paper and co-cultured on cultured medium. After 3 days, the callus was transferred to the cultured medium with 250 mg/L cephalosporins until the new callus appeared. The callus identified *PbCCT5* successfully knockdown using primers listed in Table S1 were used for subsequent RIP experiments.

RNA binding protein immunoprecipitation (RIP)

Nucleic acid and protein complexes were extracted from transgenic calluses of the pear 'Zhongai 1' [(*Pyrus ussuriensis* × *communis*) × spp.]. The callus was ground in liquid nitrogen, and then buffer A (10 mM Tris-HCl pH 8.0, 10 mM $MgCl_2$, 400 mM sucrose, 5 mM β-mercaptoethanol, 0.1 mM PMSF) was added and the mixture was vortexed for 30 s, incubated on ice for 5 min, and centrifuged at 1900 *g* for 20 min at 4℃. The precipitate was resuspended in buffer B (10 mM Tris-HCl pH 8.0, 10 mM $MgCl_2$, 250 mM sucrose, 1% [w/v] Triton-X-100, 5 mM β-me, 0.1 mM PMSF) with vortexing for 30 s and centrifuged at 11,000g for 10 min at 4℃. The precipitate was then resuspended in buffer C (10 mM Tris-HCl pH 8.0, 2 mM $MgCl_2$, 1.7 M sucrose, 0.15% w/v Triton-X-100, 5 mM β-mercaptoethanol, 0.1 mM PMSF) with vortexing for 30 s and centrifuged at 16000 g centrifugation for 60 min at 4℃. Finally, the precipitate was resuspended in buffer D (50 mM Tris-HCl pH 8.0, 10 mM EDTA pH 8.0, 1% [w/v] SDS, 0.2 mM PMSF) with vortexing for 30 s and then subjected to ultrasonic breakage at 30% intensity four times for 10 s each at 1-min intervals. The supernatant was transferred into a fresh Eppendorf tube for further RIP, which was performed following the manufacturer's protocol (Bimake Bio, B23201). The final supernatant was used for RT-qPCR analysis with the primers listed in Table S1.

Bombardment

N.benthamiana leaves were placed in a 9 cm petri dish, and the petioles were wrapped in paper soaked in water to preserve moisture. Then, 10 μL of *p35S::PbPTB3-GFP* encoding plasmid (1000 μg/μL) were mixed with 4 μL spermidine (100 mM), 10 μL

$CaCl_2$ (2.5 M) and 6 µL gold particles followed by vortexing for 10 min. The particles were rinsed with 70% ethanol for 2 times and then re-suspended in pure ethanol. Gold particles loaded with *p35S::PbPTB3-GFP* encoding plasmid were bombarded onto *hpNbCCT5-*, *hpNbCCT7-*, or *hpNbCCT8-* transgenic silenced and the wildtype tobacco leaves. Bombarded *N.benthamiana* leaves were kept under moisture in darkness for 24 h and then transferred to light for 24 h. Expression of PbPTB3-GFP in single bombarded cells and its spreading to surrounding cells was observed with a laser confocal microscope (Olympus FluoView FV1000) 48 h after bombardment (Fig. S4a,b).

***N. tabacum* transformation and grafting experiment**

Transgenic and non-transgenic *N.tabacum* (*Nicotiana tabacum* var. Wisconsin 38) plantlets were tissue-cultured on MS medium with 1 mg/L indole-3-butyric acid (IBA) for 3-4 weeks and then transplanted into soil for 2-3 weeks to graft using the split grafting method (Felsenstein and Joseph, 1985). *N.tabacum* transformation and grafting experiments were performed as described previously (Duan et al., 2016). The stock and scion stem 2 cm away from the graft union were collected 2 weeks later for immunoblot of PbPTB3 and RT-qPCR analysis of *PbWoxT1* (Fig. S4c,d).

Results

PbCCT5, a chaperonin subunit epsilon protein interacts with PbPTB3

To explore the mechanism of assembly of the *PbWoxT1*-PbPTB3 RNP complex (Duan et al., 2016), PbPTB3 was employed as a bait in a yeast two-hybrid (Y2H) screen of a *P.betulaefolia* phloem cDNA library. PbPTB3 was found to bind to two overlapping domains (aa 103-501 and aa 121-416) of a predicted subunit epsilon of chaperonin T-complex protein 1 (XM_009360981.2, Fig. S5a). A full-length cDNA sequence encoding a protein homologous to XM_009360981.2 cloned from *Pyrus betulaefolia* cDNA was found to be homologous also to the gene for T-complex protein 1 subunit epsilon (GWHAAYT025403) in the available DNA genome of the pear cultivar 'DangshanSu Li' (*P. bretschneideri* Rehd). Sequence alignment analysis indicates that the cloned DNA encodes a protein with a homeodomain motif typically present in chaperonins and sharing 77% sequence homology with CCT5 proteins of *Arabidopsis thaliana*, *Homo sapiens*, *Bos taurus* and *Saccharomyces cerevisiae* (Fig. S5b); hence,

the chaperonin subunit epsilon protein encoded by the cloned DNA is homologous to CCT5 and here referred to as PbCCT5 in the following.

Phloem mobile RNP complexes are loaded into the sieve elements (SE) from companion cells (CC) in phloem. To investigate the role of *PbCCT5* mRNA and PbCCT5 protein in the selective trafficking of the *PbWoxT1*-PbPTB3 RNP complex, we first investigated the localizations of *PbCCT5* mRNA and PbCCT5 protein in the phloem. *In situ* hybridization analysis applied to stem sections of one-year-old *P. betulaefolia* shows that *PbCCT5* mRNA is mainly localized in the phloem of the stem (Fig. 1a and 1b). For the localizations of PbCCT5 protein, the phloem of *P. betulaefolia* stem (Fig. S1), which was easily specific dissected as previously established method (Duan et al., 2016), was used for immunogold transmission electron microscopy. Consistently, also the PbCCT5 protein is localized in the phloem as shown by immunocolloidal gold staining with PbCCT5 polyclonal antibody (Fig. 1c). Tissue-specific expression analysis shows that *PbCCT5* is expressed in all tissues, including root, leaf and meristem in *P. betulaefolia* (Fig. 1d). These results suggest that the PbCCT5 protein is present in all tissues, especially in leaf and stem, and functions in all organs of the plant.

Silencing of *PbCCT5* reduces the movement of *PbWoxT1*-PbPTB3 RNP complex from root to shoot

Hairy root stable transformation system is also called cut-dip-budding (CDB) delivery system using *Agrobacterium rhizogene* to inoculate explants, generating stable transformed roots (Meng et al., 2019; Cao et al., 2022). To determine if PbCCT5 facilitates long-distance trafficking and symplastic unloading of PbPTB3, we stably co transformed the hairy roots of 3-week-old three-true-leaf *P. betulaefolia* seedlings for *SUC2* promoter-driven (Imlau et al., 1999) overexpression of GFP-fused PbPTB3 (*pSUC2::GFP-PbPTB3*) together with a *35S* promoter-driven *PbCCT5* hairpin construct (*p35S:hpPbCCT5*) aiming to silence *PbCCT5* (Fig. 2a and S6a). After co transformation, the hairy roots showed that *GFP-PbPTB3* was overexpressed and meanwhile the expression level of *PbCCT5* was successfully down-regulated, indicating that the new generation root were successfully stably transformed (Fig. 2b, S6a and S6b). Importantly, the expression levels of *PbCCT5* transcript and PbCCT5 protein that are expressed in root, hypocotyl and leaves (before transformation) were strongly reduced in their expression level in all the three tissues after transformation (Fig. 2b). And apart from the hairy roots, *GFP-PbPTB3* mRNA was not detected by

RT-PCR neither in the hypocotyl nor in the leaves, indicating that the hairy root was indeed stably transformed with *GFP-PbPTB3*, and the mobility of *GFP-PbPTB3* mRNA from transformed hairy root to the shoot was significantly reduced (Fig. 2b). At this time, we removed the true leaves of the *P. betulaefolia* seedlings to allow new true leaves to grow (Fig. S2a). Two weeks after removing true leaves and emergence of new leaves, GFP-PbPTB3 was detected by α-GFP monoclonal antibody in the new leaves as well as in the hairy root thus indicating systemic movement of GFP-PbPTB3 from the hairy root (Fig. 2c). Importantly, the GFP-PbPTB3 signal in the new leaves was significantly weaker in seedlings expressing GFP-PbPTB3 together with *hpPbCCT5* as compared to control seedlings expressing GFP-PbPTB3 together with the empty vector (EV) control (Fig. 2c and S6c), thus indicating a role of PbCCT5 in phloem mediated long-distance movement of GFP-PbPTB3. Using the same experimental setup, we also examined the mobility of free GFP. However, GFP encoded by empty vector and expressed by transcription from the *SUC2* promoter just like GFP-PbPTB3 showed no difference in mobility from hairy root to new leaves in the presence or absence of *hpPbCCT5* (Fig. S6d), indicating that the determinant that requires PbCCT5 for GFP-PbPTB3 mobility is in PbPTB3 and not in GFP. In addition, in stably transgenic hairy root plants expressing GFP-PbPTB3 construct alone, girdling the phloem of the stem interfered with GFP-PbPTB3 mobility from the hairy root to new leaves despite of a high expression level of GFP-PbPTB3 detected in the hairy roots thus suggesting that the movement of GFP-PbPTB3 from hairy roots to new leaves occurs via the phloem (Fig. 2c). CFDA applied to the hairy roots led to fluorescence in the new leaves, which confirms the existence of systemic transport from the hairy root to the new leaf in the phloem (Fig. S2b). Importantly, transformation of *pSUC2::GFP-PbCCT5* into seedling hairy roots of *P. betulaefolia*, led to detection of the 86-kDa GFP-PbCCT5 fusion protein in the hairy roots but not in new leaves (Fig. 2d), thus indicating that unlike GFP-PbPTB3, PbCCT5 lacks systemic mobility from root to shoot.

Following the demonstration that PbCCT5 facilitates root-to-shoot trafficking of the RNA-binding protein PbPTB3, we wanted to know if PbCCT5 also facilitates the trafficking of *PbWoxT1* in the phloem. Applying a similar approach as above, hairy roots were transformed for expression of *pSUC2::GFP-PbWoxT1* together with either *p35S:hpPbCCT5* or empty vector (Fig. 2e and S2a). Successful stable transformation of hairy roots was confirmed by PCR using primers homologous to the specific promoter sequences (Fig. S6e and S6f). Moreover, RT-PCR assays demonstrated the

expression of *GFP-PbWoxT1* specifically in the hairy roots but not in the hypocotyl nor in the leaves (Fig. 2f). As in the previous experiment (Fig. 2b), expression of *p35S:hpPbCCT5* led to the successful down-regulation of *PbCCT5* transcript and protein levels in all the three tissues (Fig. 2f and S6g). Interestingly, in seedlings expressing *GFP-PbWoxT1* together with *hpPbCCT5,* the mobility of *GFP-PbWoxT1* from hairy root to the new leaf was significantly reduced as compared to seedlings expressing *GFP-PbWoxT1* together with EV (Fig. 2g). Similar as already shown for PbPTB3, phloem girdling prevented the movement of *GFP-PbWoxT1* from hairy roots to the new leaves as shown by the absence of any *GFP-PbWoxT1* accumulation in phloem-girdled plants of transgenic lines expressing only *GFP-PbWoxT1* in the hairy roots (Fig. 2g). Together, these observations suggest that the long-distance trafficking of both PbPTB3 and *PbWoxT1* depends on PbCCT5 and that this trafficking occurs via the phloem. Based on the previous conclusion that PbPTB3 forms an RNP with *PbWoxT1* (Duan et al., 2016), our observations suggest a role of PbCCT5 in the mobility of the *PbWoxT1*-PbPTB3 RNP complex from root to shoot.

Sequential PbCCT complex enhances PbPTB3 stabilization and *PbWoxT1*-RNP complex binding

CCT is a cytoplasmic chaperonin in eukaryotes, consisting of eight paralogous subunits (CCT1 to CCT8) (Frydman, 2001). The full-length sequence of each PbCCT subunit (around 1500 bp) was cloned from cDNA of *P. betulaefolia* leaf with specific primers (Table S1) and confirmed by Sanger sequencing (Fig. S7a). Sequence alignments showed that all eight subunits contain conserved domains characteristic of chaperonins, with a mutual sequence identity of ~40% (Fig. S7b). Using phylogenetic analysis of the eight CCT subunits in *Arabidopsis thaliana*, *Homo sapiens*, *Bos taurus* and *Saccharomyces cerevisiae*, we classified the *Pyrus betulaefolia* CCT subunits into PbCCT1 to PbCCT8 (Fig. S8). Tissue-specific expression analysis of each PbCCT subunit show that they all owned the same tissue-specificity and were expressed in all tissues, including root, leaf and meristem in *P. betulaefolia* (Fig. S9). To identify other PbCCT subunits that may interact with PbPTB3 beyond PbCCT5, we performed yeast two-hybrid (Y2H) and bimolecular fluorescence complementation (BiFC) assays (Methods S1). The results show that in addition to PbCCT5, also PbCCT6 and PbCCT8 interact with PbPTB3, whereas subunits PbCCT1, PbCCT2, PbCCT3, PbCCT4 and PbCCT7 do not (Fig. 3a and S10). Among the four RNA recognition motif (RRM)

domains of PbPTB3, RRM1 was identified to interact with subunits PbCCT5 and PbCCT6, RRM3 interacted with PbCCT5 only, and RRM4 interacted with PbCCT5, PbCCT6 and PbCCT8, whereas RRM2 interacted with none of the PbCCT subunits (Fig. 3b). These results indicate that subunits PbCCT5, PbCCT6 and PbCCT8 interact with PbPTB3 by recognizing the RRM1, RRM2 and RRM4 domains. Additional yeast two-hybrid assays indicate that each PbCCT subunit has the capacity to interact with three other specific subunits (Fig. 3c). Similar results were obtained by BiFC assays. These also indicated that the interactions between these PbCCT subunits occur in the cytoplasm (Fig. S11). Permutation analysis revealed that the eight subunits form a ring in two adjacent pairs, whereby the clockwise order of subunits in each ring is PbCCT1, PbCCT4, PbCCT2, PbCCT5, PbCCT7, PbCCT8, PbCCT6, PbCCT3 (Fig. 3d). The above results allowed us to conclude that the eight PbCCT subunits are arranged in an ordered complex by which PbCCT5, PbCCT6 and PbCCT8 encapsulate PbPTB3 in the central cavity by recognizing the RRM1, RRM2 and RRM4 domains of PbPTB3.

To elucidate whether the PbCCT complex enhances the stability of PbPTB3, we performed a previously established *in vitro* protease sensitivity assay (Freund et al., 2014) in which we tested the stability of purified PbPTB3 from *E.coli* in the presence and absence of the purified PbCCT subunits. PbPTB3 was treated with protease K and detected by immunoblot analysis with PbPTB3-specific antibody. Protease treatment of PbPTB3 in the presence of subunits PbCCT1 to PbCCT7 or in the presence of PbCCT8 alone led to PbPTB3 degradation within 2 min, whereas PbPTB3 remained stable for 6 min when all eight subunits were present (Fig. 4a). These observations indicate that the PbCCT complex is able to protect PbPTB3 degradation by protease K and that all PbCCT subunits are necessary for this effect. PbPTB3 also remained detectable after 6 min of PK treatment when incubated in presence of the PbCCT complex purified from total protein of *P. betulaefolia* whereas it was degraded (within 2 min) in the absence of the PbCCT complex or in the presence of denatured PbCCT complex treated with 6 M Gn-HCl prior to incubation (Fig. 4b and S3a). As expected, actin, a confirmed substrate of CCT (Freund et al., 2014), also showed resistance against proteinase K. Unlike PbPTB3, bovine serum albumin (BSA) does not interact with PbCCT (Fig. S3b) and also showed no resistance against degradation by PK treatment when incubated with PbCCT in same molar ratio as PbPTB3. Taken together, these results show that the PbCCT complex has the capacity to protect PbPTB3 and

other substrates against protease digestion, which is consistent with the role of PbCCT as a chaperone for PbPTB3.

To test whether PbCCT facilitates the assembly of the *PbWoxT1*-PbPTB3 RNP complex, we performed RNA pulldown assays using purified PbPTB3 and a previously characterized *PbWoxT1* mRNA which was attached to the magnetic bead using streptomycin (Duan et al., 2016). In RNA pulldown assays, PbPTB3 was able to bind the *PbWoxT1* mRNA, but was unable to bind the mRNA after denaturation in the presence of 6 M Gn-HCl. However, the binding of the denatured PbPTB3 to the *PbWoxT1* mRNA fragment was restored in the presence of the PbCCT complex (Fig. 4c). Similarly, the relationship of PbCCT complex to the *PbWoxT1*-PbPTB3 RNP complex was verified by RNA electrophoretic mobility-shift assays (REMSAs) using purified PbPTB3 and a previously characterized *PbWoxT1* mRNA fragment (bp 309-695) shown to interact with PbPTB3 (Duan et al., 2016; Methods S1). We found that PbPTB3 was able to bind the *PbWoxT1* mRNA fragment, but was unable to bind the mRNA fragment upon denaturation in the presence of 6 M Gn-HCl. However, the binding of the denatured PbPTB3 to the *PbWoxT1* mRNA fragment was restored in the presence of the PbCCT complex (Fig. S3c). In addition, western blot analysis showed that denatured PbPTB3 was insoluble and unable to enter the gels, whereas denatured PbPTB3 entered the gel in the presence of PbCCT (Fig. S3c). Taken together, these results provide evidence indicating that PbCCT has the capacity to restore the RNA-binding activity of denatured PbPTB3 *in vitro*. In addition, pear cambium calluses transformed with *p35S:hpPbCCT5* were used for an RNA-binding protein immunoprecipitation (RIP) with anti-PbPTB3 antibody, verifying the influence of the PbCCT complex on PbPTB3 binding to *PbWoxT1 in vivo*. In this assay, the abundance of *PbWoxT1* in the PbPTB3 precipitate was significantly lower in *hpPbCCT5 RNAi* silenced callus-lines as compared to the control (WT) (Fig. 4d and 4e), indicating that the PbCCT complex facilitates PbPTB3 binding of *PbWoxT1 in vivo*. Taken together, the results allowed us to conclude that PbCCT accounts for PbPTB3 stabilization as well as for PbPTB3-associated RNP complex assembly in *P. betulaefolia.*

CCT complex affects PbPTB3 intercellular mobility in *Nicotiana benthamiana* and systemic trafficking of *PbWoxT1*-PbPTB3 RNP complex in *Nicotiana tabacum*

To understand whether (a) specific PbCCT subunit(s) or the whole PbCCT complex has a general function in *PbWoxT1*-PbPTB3 RNP trafficking, we generated

transgenic *Nicotiana benthamiana* lines in which the expression of individual CCT subunits was reduced by expression of 35S-driven and CCT subunit-specific hairpin constructs (*hpNbCCT5*, *hpNbCCT7* and *hpNbCCT8*) (Fig. S4a). Tissue specific RT-qPCR analysis showed that the three CCT subunits are commonly expressed together in various *N. benthamiana* tissues including root, stem, mesophyll, vein and meristem, and, therefore, may cooperate in the same tissues (Fig. S12). The effect of silencing CCT subunit expression on *PbWoxT1*-PbPTB3 RNP trafficking was assayed by biolistic bombardment assays to detect the intercellular mobility efficiency of GFP-PbPTB3 (Fig. S4b). In these experiments GFP-PbPTB3 showed a mobility efficiency of 17% (n=137) from bombarded cells to adjacent cells in WT leaves, whereas its mobility efficiency was down-regulated to 3% (n=152), 0.8% (n=126) and 1% (n=149) in the leaves of *hpNbCCT5*, *hpNbCCT7* and *hpNbCCT8* transgenic lines, respectively. In contrast to GFP-PbPTB3, free GFP showed a similar mobility in either WT (28%, n=129) or the transgenic *hpNbCCT5* (25%, n=135), *hpNbCCT7* (24%, n=118), and *hpNbCCT8* (25%, n=126) lines (Fig. 5a and 5b). These results indicate that the silencing of both NbCCT5 and NbCCT8, which bind to PbPTB3, and NbCCT7, which does not bind to PbPTB3, significantly decreased the efficiency of PbPTB3 cell-to-cell movement in epidermal cells of *N. benthamiana*.

To further verify the capacity of NtCCT5, NtCCT7, NtCCT8 to support PbPTB3 systemic movement, we transformed a previously established *Nicotiana tabacum* line stably co-expressing *pSUC2::PbPTB3-mCherry* and *p35S::GFP-PbWoxT1* (Duan et al., 2016) individually with *hpNtCCT5*, *hpNtCCT7*, *hpNtCCT8* or empty vector as control (Fig. 5c). Three independent lines were produced for each construct (Fig. S4c). The stocks of the resulting lines were then grafted with wild-type *N. tabacum* scions (Fig. S4d). Immunoblot analysis of the scions showed a 76-kDa band representing PbPTB3-mCherry in the scions grafted onto stocks transformed with empty vector whereas this band was rarely detectable in scions grafted onto stocks of lines in which the individual NtCCTs were silenced (Fig. 5d). *PbWoxT1* mRNA on the RNP complex was detected by using RT-qPCR with *GFP-PbWoxT1*-specific primers only in experiments using transgenic stock. Importantly, the results show that the relative abundance of *GFP-PbWoxT1* in the WT scions grafted onto stocks of *NtCCT5*, *NtCCT7* or *NtCCT8* silencing lines was significantly lower than in the WT scions grafted onto the control stocks expressing the empty vector (Fig. 5e; Table 1). Taken together, the results indicate that CCT complex promotes long-distance trafficking of *PbWoxT1*-

PbPTB3 RNP complex by promoting PbPTB3 stability and intercellular mobility in *Nicotiana* plants.

Discussion

Cofactors are essential participants in the binding of polypyrimidine binding protein to mRNAs showing long-distance trafficking in the phloem (Xoconostle-C et al., 1999; Ham et al., 2009). Therefore, we decided to use PbPTB3 as bait to search for possible interacting proteins. We identified the chaperonin protein PbCCT5 as one such protein by conserved domain analysis and sequence alignment (Fig. S5). PbCCT5, like the homologous CCT5 proteins in animals and microorganisms, is a member of an eight-subunit polycyclic complex, CCT, which encapsulates substrate proteins inside a central cavity (Hartl et al., 2011). The structural variability of the apical domain of each CCT subunit confers substrate binding specificity: for instance, tubulin mainly binds to CCT2, CCT4 and CCT6 (Kalisman et al., 2013; Joachimiak et al., 2014), the Box1 domain of the tumor suppressor VHL binds to CCT1 and CCT7 (Spiess et al., 2006), and the leukemia fusion tumor protein AML1-ETO binds to CCT2, CCT3, CCT4, CCT6 and CCT7 (Roh et al., 2016). In our study, PbPTB3 is a newly identified substrate of the PbCCT complex, of which RRM1, RRM3 and RRM4 domains interact directly with PbCCT5, PbCCT6 and PbCCT8 (Fig. 3a and 3b). The subunits of PbCCT are organized in a distinctive arrangement (Fig. 3c and 3d), which is in good agreement with the TRiC model in *Saccharomyces cerevisiae* (Leitner et al., 2012), but slightly different from that of *Homo sapiens* and *Bos taurus* CCT complexes (Llorca et al., 1999; Munoz et al., 2011; Cong et al., 2012). Here we demonstrate that the chaperonin CCT binds different substrates with strong interaction specificity.

To investigate the effects of the PbCCT5 on the long-distance trafficking of the RNP complex, we used the hairy root stable transformation system reported previously (Meng et al., 2019; Cao et al., 2022). As we did not detect any trafficking of PbCCT5 from hairy roots to new leaves (Fig. 2d), we speculate that the PbCCT complex plays a role specifically at the source, but does not take part in the long-distance trafficking of the RNP complexes through the phloem. We also establish that the trafficking from hairy roots to new leaves of both PbPTB3 and *PbWoxT1* is reduced when PbCCT5 is

silenced (Fig. 2 and S6). Although hairy root is a sink tissue under normal conditions, the removal of plant leaves and shoot apex in our experiments likely converted the root system into a source able to transport RNA and protein signals to the new leaves (Fig. S2a). Following loading on hairy roots the symplastic transport tracer CFDA occurred in the new leaves thus confirming transport flow from hairy root to new leaf (Fig. S2b). Consistently, we observed that the expression of *hpPbCCT5* as the silencing trigger caused *PbCCT5* silencing not only in the transfected hairy root but also in the hypocotyl and new leaf, which confirms the hairy roots as a source tissue in our experiments and also suggests that *hpPbCCT5* or derived siRNAs are mobile and thereby may have enhanced the reduction in *PbWoxT1* and PbPTB3 systemic transport. Despite these specific experimental conditions, we infer that PbCCT5 plays a role in PbPTB3 stabilization and RNP assembly at the source but does not take part in the long-distance trafficking of RNP complexes from source to sink.

The main function of chaperonin binding to a substrate is to fold the substrate protein, in a reaction that is catalyzed by ATP binding and hydrolysis (Klumpp et al., 1997; Ditzel et al., 1998; Horwich, 2014). Folding is an important step in the transformation of a polypeptide chain from an inactive to an active state. This process controls protein homeostasis in cells, dictates the folded conformation of proteins, and regulates the transmembrane flow between cells (Horwich et al., 2007; Hartl et al., 2011). Our research demonstrated that the PbCCT complex interacted with PbPTB3 and facilitated the formation of the *PbWoxT1*-PbPTB3 RNP complex (Fig. 4). In previous studies, the CCT complex was reported to interact with the leukemia fusion tumor protein AML1-ETO to modulate it to bind DNA molecules (Roh et al., 2016). CCT also regulates the folding of functional proteins involved in many other biological processes, including cell cycle regulators (CDC20 and CDH1) (Camasses et al., 2003), a cancer suppressor (VHL and p53) (Feldman et al., 1999; Spiess et al., 2006) and the telomerase cofactor (TCAB1) (Freund et al., 2014). For phloem trafficking, RNP complexes assembled by trafficking mRNAs and proteins enter the STS by passing through the CC-SEPD; however, the PD permits the passage of specific molecules only if their effective hydrodynamic Stoke's radius is smaller than the size of exclusion limit

(SEL), which for the PD at the CC-SE interface applies to proteins with a molecular weight of 10~60 kDa (Stadler et al., 2005; Faulkner, 2018). However, RNP complexes previously observed in pumpkin sap (Ham et al., 2009), potato (Cho et al., 2015) and pear (Duan et al., 2016) were all far greater in size, which suggests that the assembly of each RNP complex is an important process in phloem trafficking (Lucas et al., 2013; Ham and Lucas, 2016). Thus, the observation that the CCT complex folds proteins led us to speculate that the PbCCT complex functions similar to animal CCT complexes in the binding of substrate proteins in order to fold them into conformations required for passing through PD to transport in phloem. However, further structural analysis of the PbCCT complex and of PbPTB3 may be needed to support this hypothesis.

In previous studies in plants, chaperonins were shown to facilitate cell-to-cell trafficking KNOX factors as well as the movement protein-dependent intercellular spread of viral RNA (Xu et al., 2011; Fichtenbauer et al., 2012). Our research shows that the efficiency of cell-to-cell transport of PbPTB3 in *Nicotiana benthamiana* was reduced by CCT subunit silencing (Fig. 5a and 5b). Furthermore, the trafficking of both PbPTB3 and *PbWoxT1* from stock to scion was significantly reduced in tobacco plants grafted to stock in which the tobacco CCT subunits *NtCCT5* or *NtCCT8* (which interacted with PbPTB3) or *NtCCT7* (which did not interact with PbPTB3) were silenced, compared to the unsilenced control (Fig. 5d and 5e). The same results were obtained in the F_2 generation (Table 1), which further confirmed that the CCT complex is involved in the phloem long-distance trafficking of the *PbWoxT1*-PbPTB3 complex between the stock and the scion in *N.tabacum*. The long-distance trafficking of RNP complex is completed by loading at the source tissue and unloading at the sink tissue, and the RNP complex synthesis in source is transported to the phloem through intercellular transport. According to our above study, it is speculated that the influence of CCT complex on the long-distance trafficking of RNP complex in phloem is probably caused by its influence on the intercellular movement.

In this study, we have found that the silencing of PbCCT subunits inhibited the systemically trafficking of *PbWoxT1,* which has been reported to elongate the style of flower in *N. tabacum* so as to facilitate hybridization (Duan et al., 2016). Self-

incompatibility is a pervasive barrier for fruit trees, especially in pear breeding. Longer styles of flowers increase the probability of pollen from other plants to land on the stigma and thus improve fruit setting, significantly benefiting fruit tree breeding (Li et al., 2009). Thus, in acting as a chaperone in the phloem, the CCT complex facilitates folding of RNA-binding proteins, which in turn supports the long-distance trafficking of RNA signals (like *PbWoxT1*) and their function in sink tissues, such as in flower development. Treatment of plants with nanomaterials loaded with the PbCCT complex could be a non-GMO approach to increase the transport efficiency of *PbWoxT1* in order to improve breeding.

Acknowledgements

We thank the ikann-editorial team for their language and writing assistance and suggestions. This work was supported by the National Key Research and Development Program of China (2018YFD1000103), the earmarked fund for the China Agriculture Research System (CARS-28-08) and the National Natural Science Foundation of China (32002011, 32272658) and the 2115 Talent Development Program of China Agricultural University.

Author Contributions

Shengnan Wang, Xuwei Duan, Wenna Zhang and Tianzhong Li designed experiments. Shengnan Wang performed most of the experiment and analyzed experimental data. Shengyuan Wang, Li Hao, Feng Jiang and Yi Zhang performed some experiments. Shengnan Wang, Wenna Zhang and Tianzhong Li wrote the manuscript, Manfred Heinlein and Wenna Zhang revised the manuscript. Chaoran Xu, Ling Xiang, Feng Jiang and Yunfei Yu performed some sample collections.

Data availability

All study data are included in the article text and/or figures and/or supporting information.

.

Accession numbers

PbWoxT1 (KT998806), *PbPTB3* (KT998805), *PbCCT1* (OQ092305), *PbCCT2* (OQ092306), *PbCCT3* (OQ092307), *PbCCT4* (OQ092308), *PbCCT5* (OQ092309),

PbCCT6 (OQ092310), *PbCCT7* (OQ092311), *PbCCT8* (OQ092312), *NtCCTl* (OQ092313), *NtCCT2* (OQ092314), *NtCCT3* (OQ092315), *NtCCT4* (OQ092316), *NtCCT5* (OQ092317), *NtCCT6* (OQ092318), *NtCCT7* (OQ092319), *NtCCT8* (OQ092320).

Competing interests

None declared.

References

Ahn, H.K., Yoon, J.T., Choi, I., Kim, S., Lee, H.S., and Pai, H.S. 2019. Functional characterization of chaperonin containing T-complex polypeptide-1 and its conserved and novel substrates in Arabidopsis. J Exp Bot **70,** 2741-2757.

Anna Ostendorp, Steffen Ostendorp, Yuan Zhou, Zoé Chaudron, Lukas Wolffram, Khadija Rombi, Linn von Pein, Sven Falke, Cy M. Jeffries, Dmitri I. Svergun, Christian Betzel, Richard J. Morris, Friedrich Kragler, Julia Kehr. 2022. Intrinsically disordered plant protein PARCL co-localizes with RNA in phase-separated condensates whose formation can be regulated by mutating the PLD. Journal of Biological Chemistry. Available online, 102631

Bai, C., Guo, P., Zhao, Q., Lv, Z., Zhang, S., Gao, F., Gao, L., Wang, Y., Tian, Z., Wang, J., Yang, F., and Liu, C. 2015. Protomer Roles in Chloroplast Chaperonin Assembly and Function. Mol Plant **8,** 1478-1492.

Banerjee, A.K., Chatterjee, M., Yu, Y., Suh, S.G., Miller, W.A., and Hannapel, D.J. 2006. Dynamics of a mobile RNA of potato involved in a long-distance signaling pathway. Plant Cell **18,** 3443-3457.

Camasses, A., Bogdanova, A., Shevchenko, A., and Zachariae, W. 2003. The CCT chaperonin promotes activation of the anaphase-promoting complex through the generation of functional Cdc20. Mol Cell **12,** 87-100.

Cao, X., Xie, H., Song, M., Lu, J., Ma, P., Huang, B., Wang, M., Tian, Y., Chen, F., Peng, J., Lang, Z., Li, G., Zhu, J.-K.. 2022. Cut-dip-budding delivery system enables genetic modifications in plants without tissue culture. The Innovation . doi: https://doi.org/10.1016/ j.xinn. 100345.

Cho, S.K., Sharma, P., Butler, N.M., Kang, I.H., Shah, S., Rao, A.G., and Hannapel, D.J. 2015. Polypyrimidine tract-binding proteins of potato mediate tuberization through an interaction with StBEL5 RNA. J Exp Bot **66,** 6835-6847.

Cong, Y., Schroder, G.F., Meyer, A.S., Jakana, J., Ma, B., Dougherty, M.T., Schmid, M.F., Reissmann, S., Levitt, M., Ludtke, S.L., Frydman, J., and Chiu, W. 2012. Symmetry-free cryo-EM structures of the chaperonin TRiC along its ATPase-driven conformational cycle. EMBO J **31,** 720-730.

Ditzel, L., Lowe, J., Stock, D., Stetter, K.O., Huber, H., Huber, R., and Steinbacher, S. 1998. Crystal structure of the thermosome, the archaeal chaperonin and homolog of CCT. Cell **93,** 125-138.

Duan, X., Zhang, W., Huang, J., Hao, L., Wang, S., Wang, A., Meng, D., Zhang, Q., Chen, Q., and Li, T. 2016. PbWoxT1 mRNA from pear (Pyrus betulaefolia) undergoes long-distance transport assisted by a polypyrimidine tract binding protein. New Phytol **210,** 511-524.

Faulkner, C. 2018. Plasmodesmata and the symplast. Curr Biol **28,** R1374-R1378.

Feldman, D.E., Thulasiraman, V., Ferreyra, R.G., and Frydman, J. 1999. Formation of the VHL-elongin BC tumor suppressor complex is mediated by the chaperonin TRiC. Mol Cell **4,** 1051-1061.

Felsenstein, and Joseph. 1985. CONFIDENCE LIMITS ON PHYLOGENIES: AN APPROACH USING THE BOOTSTRAP. Evolution **39,** 783-791.

Fichtenbauer, D., Xu, X.M., Jackson, D., and Kragler, F. 2012. The chaperonin CCT8 facilitates spread of tobamovirus infection. Plant Signal Behav **7,** 318-321.

Freund, Adam, Zhong, Franklin, L., Venteicher, Andrew, S., Meng, Zhaojing, Veenstra, and Timothy, D. 2014. Proteostatic Control of Telomerase Function through TRiC-Mediated Folding of TCAB1. CELL **159,** 1389-1403.

Frydman, J. 2001. Folding of newly translated proteins in vivo: the role of molecular chaperones. Annu Rev Biochem **70,** 603-647.

Ham, B.K., and Lucas, W.J. 2016. Phloem-Mobile RNAs as Systemic Signaling Agents. Annual Review of Plant Biology **68,** 173.

Ham, B.K., Brandom, J.L., Xoconostle-Cazares, B., Ringgold, V., Lough, T.J., and Lucas, W.J. 2009. A polypyrimidine tract binding protein, pumpkin RBP50, forms the basis of a phloem-mobile ribonucleoprotein complex. Plant Cell **21,** 197-215.

Hao, L., Zhang, Y., Wang, S., Zhang, W., Wang, S., Xu, C., Yu, Y., Li, T., Jiang, F., and Li, W. 2020. A constitutive and drought-responsive mRNA undergoes long-distance transport in pear (Pyrus betulaefolia) phloem. Plant Sci **293,** 110419.

Hartl, F.U., Bracher, A., and Hayer-Hartl, M. 2011. Molecular chaperones in protein folding and proteostasis. Nature **475,** 324-332.

Haywood, V., Kragler, F., and Lucas, W.J. 2002. Plasmodesmata: pathways for protein and ribonucleoprotein signaling. Plant Cell **14 Suppl,** S303-325.

Haywood, V., Yu, T.S., Huang, N.C., and Lucas, W.J. 2005. Phloem long-distance trafficking of GIBBERELLIC ACID-INSENSITIVE RNA regulates leaf development. Plant J **42,** 49-68.

Himmelspach, R., Nick, P., Schafer, E., and Ehmann, B. 1997. Developmental and light-dependent changes of the cytosolic chaperonin containing TCP-1 (CCT) subunits in maize seedlings, and the localization in coleoptiles. Plant J **12,** 1299-1310.

Horwich, A.L. 2014. Molecular chaperones in cellular protein folding: the birth of a field. Cell **157,** 285-288.

Horwich, A.L., Fenton, W.A., Chapman, E., and Farr, G.W. 2007. Two families of chaperonin: physiology and mechanism. Annu Rev Cell Dev Biol **23,** 115-145.

Huang, N.C., Luo, K.R., and Yu, T.S. 2018. Mobility of Antiflorigen and PEBP mRNAs in Tomato-Tobacco Heterografts. Plant Physiol **178,** 783-794.

Imlau, A., Truernit, E., and Sauer, N. 1999. Cell-to-cell and long-distance trafficking of the green fluorescent protein in the phloem and symplastic unloading of the protein into sink tissues. Plant Cell **11,** 309-322.

Joachimiak, L.A., Walzthoeni, T., Liu, C.W., Aebersold, R., and Frydman, J. 2014. The structural basis of substrate recognition by the eukaryotic chaperonin TRiC/CCT. Cell **159,** 1042-1055.

Kalisman, N., Schroder, G.F., and Levitt, M. 2013. The crystal structures of the eukaryotic chaperonin CCT reveal its functional partitioning. Structure **21,** 540-549.

Kehr, J., Morris, R.J., and Kragler, F. 2021. Long-Distance Transported RNAs: From Identity to Function. Annu Rev Plant Biol.

Kim, Minsung, Canio, Wynnelena, Kessler, Sharon, Sinha, and Neelima. 2001. Developmental Changes Due to Long-Distance Movement of a Homeobox Fusion Transcript in Tomato. Science.

Kitagawa, M., Wu, P., Balkunde, R., Cunniff, P., and Jackson, D. 2022. An RNA exosome subunit mediates cell-to-cell trafficking of a homeobox mRNA via plasmodesmata. Science **375,** 177-182.

Klumpp, M., Baumeister, W., and Essen, L.O. 1997. Structure of the substrate binding domain of the thermosome, an archaeal group II chaperonin. Cell **91,** 263-270.

Leitner, A., Joachimiak, L.A., Bracher, A., Monkemeyer, L., Walzthoeni, T., Chen, B., Pechmann, S., Holmes, S., Cong, Y., Ma, B., Ludtke, S., Chiu, W., Hartl, F.U., Aebersold, R., and Frydman, J. 2012. The molecular architecture of the eukaryotic chaperonin TRiC/CCT. Structure **20,** 814-825.

Li, M.F., Li, X.F., Han Zh, H., Shu, H.R., and Li, T. 2009. Molecular analysis of two Chinese pear (Pyrus bretschneideri Rehd.) spontaneous self-compatible mutants, Yan Zhuang and Jin Zhui. Plant Biol (Stuttg) **11,** 774-783.

Li, P., Ham, B.K., and Lucas, W.J. 2011. CmRBP50 Protein Phosphorylation Is Essential for Assembly of a Stable Phloem-mobile High-affinity Ribonucleoprotein Complex. Journal of Biological Chemistry **286**.

Liu, L., Li, C., Teo, Z.W.N., Zhang, B., and Yu, H. 2019. The MCTP-SNARE Complex Regulates Florigen Transport in Arabidopsis. Plant Cell **31,** 2475-2490.

Llorca, O., McCormack, E.A., Hynes, G., Grantham, J., Cordell, J., Carrascosa, J.L., Willison, K.R., Fernandez, J.J., and Valpuesta, J.M. 1999. Eukaryotic type II chaperonin CCT interacts with actin through specific subunits. Nature **402,** 693-696.

Lu, K.J., Huang, N.C., Liu, Y.S., Lu, C.A., and Yu, T.S. 2012. Long-distance movement of Arabidopsis FLOWERING LOCUS T RNA participates in systemic floral regulation. RNA Biol **9,** 653-662.

Lucas, W.J., Groover, A., Lichtenberger, R., Furuta, K., Yadav, S.R., Helariutta, Y., He, X.Q., Fukuda, H., Kang, J., Brady, S.M., Patrick, J.W., Sperry, J., Yoshida, A., Lopez-Millan, A.F., Grusak, M.A., and Kachroo, P. 2013. The plant vascular system: evolution, development and functions. J Integr Plant Biol **55,** 294-388.

Meng, D., Yang, Q., Dong, B., Song, Z., Niu, L., Wang, L., Cao, H., Li, H., and Fu, Y. 2019. Development of an efficient root transgenic system for pigeon pea and its application to other important economically plants. Plant Biotechnol J **17,** 1804-1813.

Moser, M., Schafer, E., and Ehmann, B. 2000. Characterization of protein and transcript levels of the chaperonin containing tailless complex protein-1 and tubulin during light-regulated growth of oat seedlings. Plant Physiol **124,** 313-320.

Munoz, I.G., Yebenes, H., Zhou, M., Mesa, P., Serna, M., Park, A.Y., Bragado-Nilsson, E., Beloso, A., de Carcer, G., Malumbres, M., Robinson, C.V., Valpuesta, J.M., and Montoya, G. 2011. Crystal structure of the open conformation of the mammalian chaperonin CCT in complex with tubulin. Nat Struct Mol Biol **18,** 14-19.

Nie, J., Shan, N., Liu, H., Yao, X., Wang, Z., Bai, R., Guo, Y., Duan, Y., Wang, C., and Sui, X. 2021. Transcriptional control of local auxin distribution by the CsDFB1-CsPHB module regulates floral organogenesis in cucumber. Proc Natl Acad Sci U S A **118**.

Notaguchi, M., Wolf, S., and Lucas, W.J. 2012. Phloem-mobile Aux/IAA transcripts target to the root tip and modify root architecture. J Integr Plant Biol **54,** 760-772.

Paul, A., Tiotiu, D., Bragantini, B., Marty, H., Charpentier, B., Massenet, S., and Labialle, S. 2019. Bcd1p controls RNA loading of the core protein Nop58 during C/D box snoRNP biogenesis. RNA **25,** 496-506.

R G Ferreyra and J Frydman. 2000. Purification of the cytosolic chaperonin TRiC from Bovine Testis. Methods Mol Biol. 140:153-60.

Roh, S.H., Kasembeli, M., Galaz-Montoya, J.G., Trnka, M., Lau, W.C., Burlingame, A., Chiu, W., and Tweardy, D.J. 2016. Chaperonin TRiC/CCT Modulates the Folding and Activity of Leukemogenic Fusion Oncoprotein AML1-ETO. J Biol Chem **291,** 4732-4741.

Ruiz-Medrano, R., Xoconostle-Cazares, B., and Lucas, W.J. 1999. Phloem long-distance transport of CmNACP mRNA: implications for supracellular regulation in plants. Development **126,** 4405-4419.

Spiess, C., Miller, E.J., McClellan, A.J., and Frydman, J. 2006. Identification of the TRiC/CCT substrate binding sites uncovers the function of subunit diversity in eukaryotic chaperonins. Mol Cell **24,** 25-37.

Stadler, R., Wright, K.M., Lauterbach, C., Amon, G., Gahrtz, M., Feuerstein, A., Oparka, K.J., and Sauer, N. 2005. Expression of GFP-fusions in Arabidopsis companion cells reveals non-specific protein trafficking into sieve elements and identifies a novel post-phloem domain in roots. Plant J **41,** 319-331.

Tsutsui, and Notaguchi. 2017. The Use of Grafting to Study Systemic Signaling in Plants. PLANT CELL PHYSIOL **2017,58(8),** 1291-1301.

Xoconostle-C, aacute, and Zares, B. 1999. Plant Paralog to Viral Movement Protein That Potentiates Transport of mRNA into the Phloem. Science **283,** 94-98.

Xu, X.M., Wang, J., Xuan, Z., Goldshmidt, A., Borrill, P.G., Hariharan, N., Kim, J.Y., and Jackson, D. 2011. Chaperonins facilitate KNOTTED1 cell-to-cell trafficking and stem cell function. Science **333,** 1141-1144.

Yaffe, M.B., Farr, G.W., Miklos, D., Horwich, A.L., and Sternlicht, H. 1992. TCP1 complex is a molecular chaperone in tubulin biogenesis. Nature **358,** 245-248.

Yijie, Gao, and, John, O., Thomas, and, Robert, L., and Chow. 1992. A cytoplasmic chaperonin that catalyzes β-actin folding. Cell **69,** 1043-1050.

Supporting information

Main Figures Legends

Figure 1. The localization of PbCCT5 mRNA and protein in *Pyrus betulaefolia*. Detection of *PbCCT5* transcripts by *in situ* hybridization in 8 μm cross **(a)** and longitudinal sections **(b)** of the stem of one-year-old *Pyrus betulaefolia*. Red solid lines indicate phloem cells, red dashed boxes in 10x view indicate areas of magnification used to display CC and SE in 40x view. Red arrowheads indicate *PbCCT5* transcripts detected with anti-sense probe. Sense probe of *PbCCT5* was used as a negative control for *in situ* hybridization. The 479 bp fragment recognizing 643-1122 bp of *PbCCT5* was used for *in situ* hybridization probe. A scale bar is shown in each sub-figure. In **(a)** and **(b)**, a CC-specific marker, *PbSUC2* was used as controls to indicate the localization of companion cells. Three individual plants and each individual plant included at least 10 sections were analyzed. SE, Sieve Element. CC, Companion Cell.

(c) Immunogold detection of PbCCT5 protein in ultrathin sections of phloem cells in one-year-old *P. betulaefolia* using anti-PbCCT5 polyclonal antibodies. Red dashed boxes indicate the areas of magnification. Black arrowheads indicate the locations of gold particles. A scale bar is shown in each sub-figure.

(d) RT-qPCR analysis of *PbCCT5* in different tissues of *P. betulaefolia*. *18S rRNA* was used as the internal control. The results show the mean ± SD and are based on three technical replicates.

Figure 2. Silencing of PbCCT5 inhibits PbPTB3 mobility from root to shoot in *Pyrus betulaefolia*

(a) Vector constructions used for hairy root transformation for **(b)** and **(c)** in two-week-old *P. betulaefolia*.

(b) Standard RT-PCR analysis of *PbPTB3* and *PbCCT5* levels in the root, hypocotyl and leaves of seedlings before transformation, and also in the hairy root, hypocotyl and new leaf of seedlings 28 dpi after transformation for *GFP-PbPTB3* expression and *hpPbCCT5*-mediated *PbCCT5* silencing. *18S rRNA* was used as the internal control in the analysis of mRNA abundance. The lower part of the figure shows the levels of PbCCT5 protein expression as detected by immunoblot analysis (WB) using anti-PbCCT5 polyclonal antibody. CBB, coomassie brilliant blue stained proteins.

(c) GFP-PbPTB3 in pCAMBIA1305.1 trafficking from hairy root to new leaf as indicated by immunoblot analysis using anti-GFP monoclonal antibodies. The hairy root was transformed with empty vector (EV) or vector harboring *hpPbCCT5* for *PbCCT5* silencing. The relative expression levels shown below each protein band were normalized to the total protein. EV, pFGC5941 empty vector; CBB, coomassie brilliant blue stained protein; 12 independent transgenic seedlings as 12 biological replicates for each combination were used for the analysis here, #1, #2, and #3 refer to three transformant pools and each pool including four independent transgenic seedlings with similar *PbCCT5* silencing levels.

(d) 28 d after transformation, absence of trafficking of GFP-PbCCT5 fusion protein from GFP-PbCCT5 transformed hairy root to new leaf detected by immunoblot analysis using anti-GFP monoclonal antibodies. The relative expression levels were normalized to the total protein. CBB, coomassie brilliant blue stained protein; WT, non-transformed control; 3 independent transgenic seedlings as 3 biological replicates for each combination were used for the analysis here, #1, #2, and #3 indicate three transgenic seedlings as 3 biological replicates.

(e) Vector constructions used for hairy root transformation for **(f)** and **(g)** in two-week-old *P. betulaefolia*.

(f) Standard RT-PCR analysis showing the relative expression levels of overexpressed *GFP-PbWoxT1* and endogenous *PbCCT5* in tissues of non-transformed plants in comparison to transformed plants expressing *PbWoxT1* and *hpPbCCT5* in the hairy root. *18S rRNA* was used as the internal control in the analysis of mRNA abundance.

The lower part of the figure shows the level of expression of PbCCT5 protein detected with anti-PbCCT5 polyclonal antibodies. CBB, coomassie brilliant blue stained protein. **(g)** RT-qPCR analysis of the effect of *PbCCT5* silencing in transformed hairy roots on *GFP-PbWoxT1* trafficking from transformed hairy roots (R) to new leaves (L). *18S rRNA* was used as the internal control in the analysis of mRNA abundance. 12 independent transgenic seedlings were used for 12 biological replicates. Results for each biological replicate are based on three technical replicates represented by mean ± SD. Data for relative *GFP-PbWoxT1* abundance in hairy root versus new leaf were analyzed using unpaired two-tailed Student's *t*-test (*P<0.05; **P<0.01) with SPSS. EV, pFGC5941 empty vector; R, hairy root; L, new leaf.

Figure 3. Interactions between PbCCT subunits and with PbPTB3.

(a) Yeast two-hybrid analysis showing the interaction between PbCCT subunits and PbPTB3. Empty vectors were used as negative controls.

(b) Interaction between PbCCT5, PbCCT6, PbCCT8 subunits and four PbPTB3 fragments carrying specific RNA recognition motif (RRM) domains. Empty vectors were used as negative controls. aa: amino acid.

(c) Pairwise analysis of interactions between PbCCT subunits. The interaction between SV40 and P53 was used as positive control and empty vectors were used as negative control.

(d) Structural model of the eight PbCCT subunits and four PbPTB3 RRM domains. Different colors indicated different subunits.

Figure 4. PbCCT complex facilitates PbPTB3 stabilization and *PbWoxT1* binding.

(a) All eight PbCCT subunits participate in PbPTB3 stabilization, as indicated by a protease sensitivity assay. Anti-PbPTB3 polyclonal antibodies were used for PbPTB3 detection. PK, proteinase K.

(b) The purified *in vivo* PbCCT complex participates in PbPTB3 stabilization, as indicated by a protease sensitivity assay. PbPTB3 is degraded in the absence of PbCCT ("Non-PbCCT") or in the presence of PbCCT denatured by 6 M guanidium-hydrochloride (Gn-HCl). Anti-PbPTB3 and anti-PbCCT8 polyclonal antibodies were used for the detection of PbPTB3 and PbCCT8, respectively; PbActin and BSA were

used as positive and negative controls, respectively, and were detected with specific monoclonal antibodies. PbCCT denatured by 6 M Gn-HCl was used as a control for the folded PbCCT complex.

(c) PbCCT restores RNA binding activity of 6 M Gn-HCl-treated PbPTB3. RNA pulldown assays were performed using biotin-labeled *PbWoxT1* RNA and PbPTB3 fused to GST. Unfused GST was used as a negative control. Immunoblotting was performed with anti-PbPTB3 polyclonal antibodies. RT-PCR was performed with specific primers for *PbWoxT1*.

(d) Standard PCR analysis of the relative *PbCCT5* expression levels in wild type and *hpPbCCT5 RNAi* callus lines. *18S rRNA* was used as the internal control in the analysis of mRNA abundance. #1, #2, and #3, indicate three transgenic calluses as 3 biological replicates. **(e)** *PbCCT5* silencing inhibits the ability of PbPTB3 to bind *PbWoxT1*. Levels of *PbWoxT1* associated with PbPTB3 upon co-immunoprecipitation with PbPTB3 antibodies. *18S rRNA* was used as the internal control for the RT-qPCR used to analyze *PbWoxT1* abundance. IP, immunoprecipitation. #1, #2, and #3, indicate three transgenic calluses as 3 biological replicates. The results for each replicate are represented by the mean ± SD of three technical replicates. Data were analyzed using unpaired two-tailed Student's t-test (**P<0.01) with SPSS software.

Figure 5. General function of PbCCT and NtCCT in RNP trafficking in *Nicotina benthamiana* and *Nicotina tabaccum*.

(a) Analysis of intercellular movement of GFP-PbPTB3 in *N. benthamiana* leaves of wild type and *hpNbCCT5, hpNbCCT7* and *hpNbCCT8* transgenic silenced lines. The number at top right means the cells number of GFP-PbPTB3/GFP moved to surrounding in total bombardment cells amount. The asterisks mark individual cells.

(b) Statistical analysis of GFP-PbPTB3/GFP mobile frequency in wild type and *hpNbCCT5, hpNbCCT7* and *hpNbCCT8* transgenic silenced lines.

(c) Vector construction used in transgenic *N.tabaccum*.

(d) Analysis of PbPTB3 protein trafficking from multiple transgenic *N.tabaccum* stock to wild-type scion. Immunoblot analyses were performed using anti-PbPTB3 polyclonal antibodies to detect the quantity of the PbPTB3-mCherry fusion protein transferred. The relative expression levels were normalized to the total protein. CBB, coomassie brilliant blue stained protein.

(e) Analysis of *PbWoxT1* mRNA trafficking from multiple transgenic *N.tabaccum* stock to wild-type scion. RT-qPCR was performed to detect the quantity of *PbWoxT1* mRNA transferred. *18S rRNA* was used as the internal control. The results show the mean ± SD and are based on three technical replicates. Data were analyzed using unpaired two-tailed Student's *t*-test (**P<0.01).

(d-e) Data are for co-overexpression *N.tabaccum* lines transformed with *pSUC2::PbPTB3-mCherry* and *p35S::GFP-PbWoxT1* (Co-OE) together with *hpNtCCT* subunits construction. WT, wild type; EV: Co-OE + pFGC5941 empty vector; *hpNtCCT5*: Co-OE + *hpNtCCT5*; *hpNtCCT7:* Co-OE + *hpNtCCT7*; *hpNtCCT8:* Co-OE + *hpNtCCT8*. #1, #2, and #3 refer to three independently grafted plants used as biological replicates.

Table 1. PbPTB3 and *PbWoxT1* trafficking in *N.tabaccum* grafting system

Grafting (Scion/Rootstock)	*PbWoxT1*				PbPTB3			
	#1	#2	#3	Percent	#1	#2	#3	Percent
	Transport / Total	Transport / Total	Transport / Total		Transport / Total	Transport / Total	Transport / Total	
WT/Co-OE+EV	3/5	5/7	5/7	68%	4/5	5/7	5/7	74%
WT/Co-OE+*hpNtCCT5 RNAi*	2/7	1/5	0/6	17%	1/7	1/5	0/6	11%
WT/Co-OE+*hpNtCCT7 RNAi*	0/7	1/7	1/5	11%	1/7	1/7	0/5	11%
WT/Co-OE+*hpNtCCT8 RNAi*	0/6	1/7	2/5	17%	0/6	0/7	2/5	11%

#1, #2, and #3 refer to three independently grafted plants used as biological replicates.

Figure 1

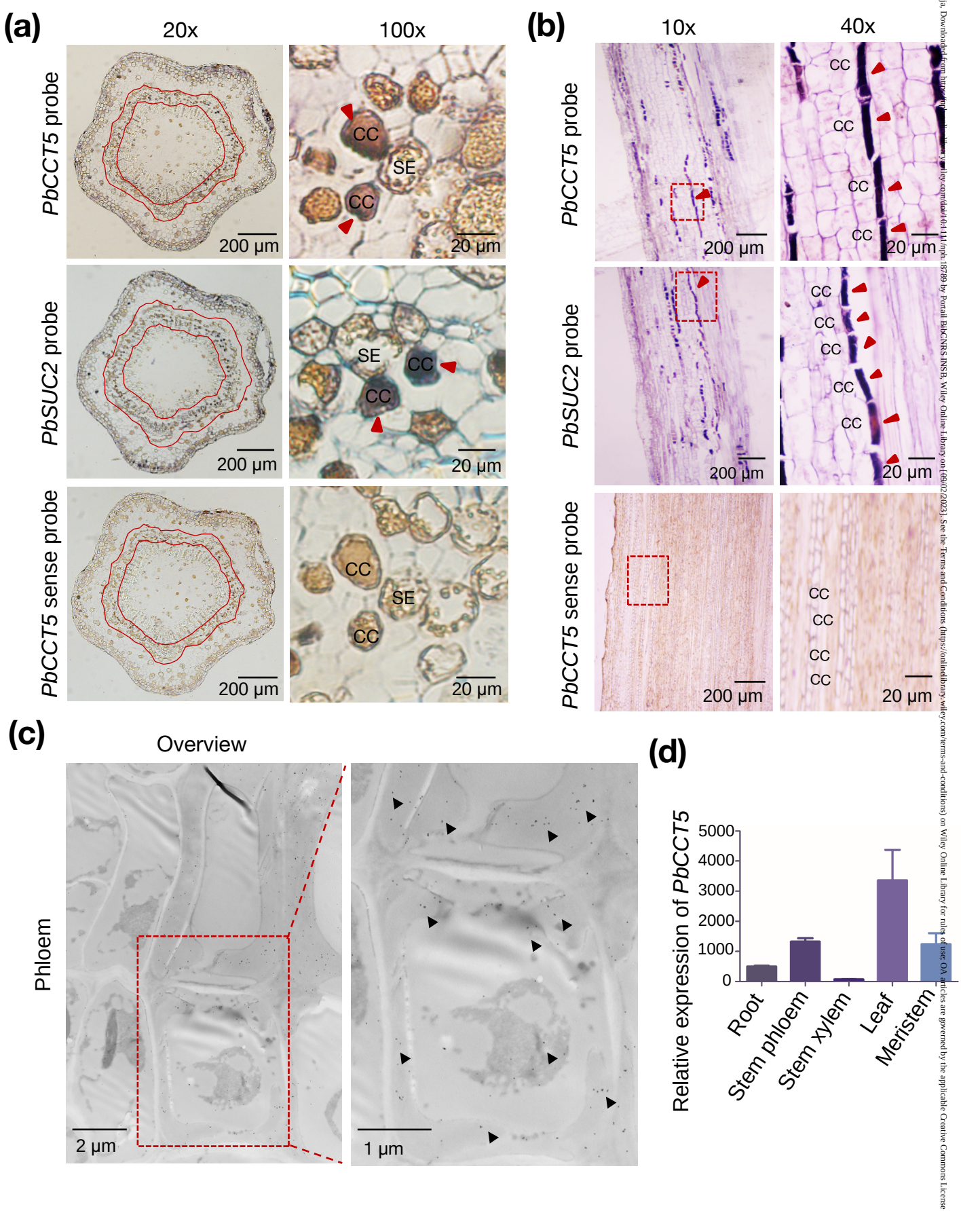

Figure 2

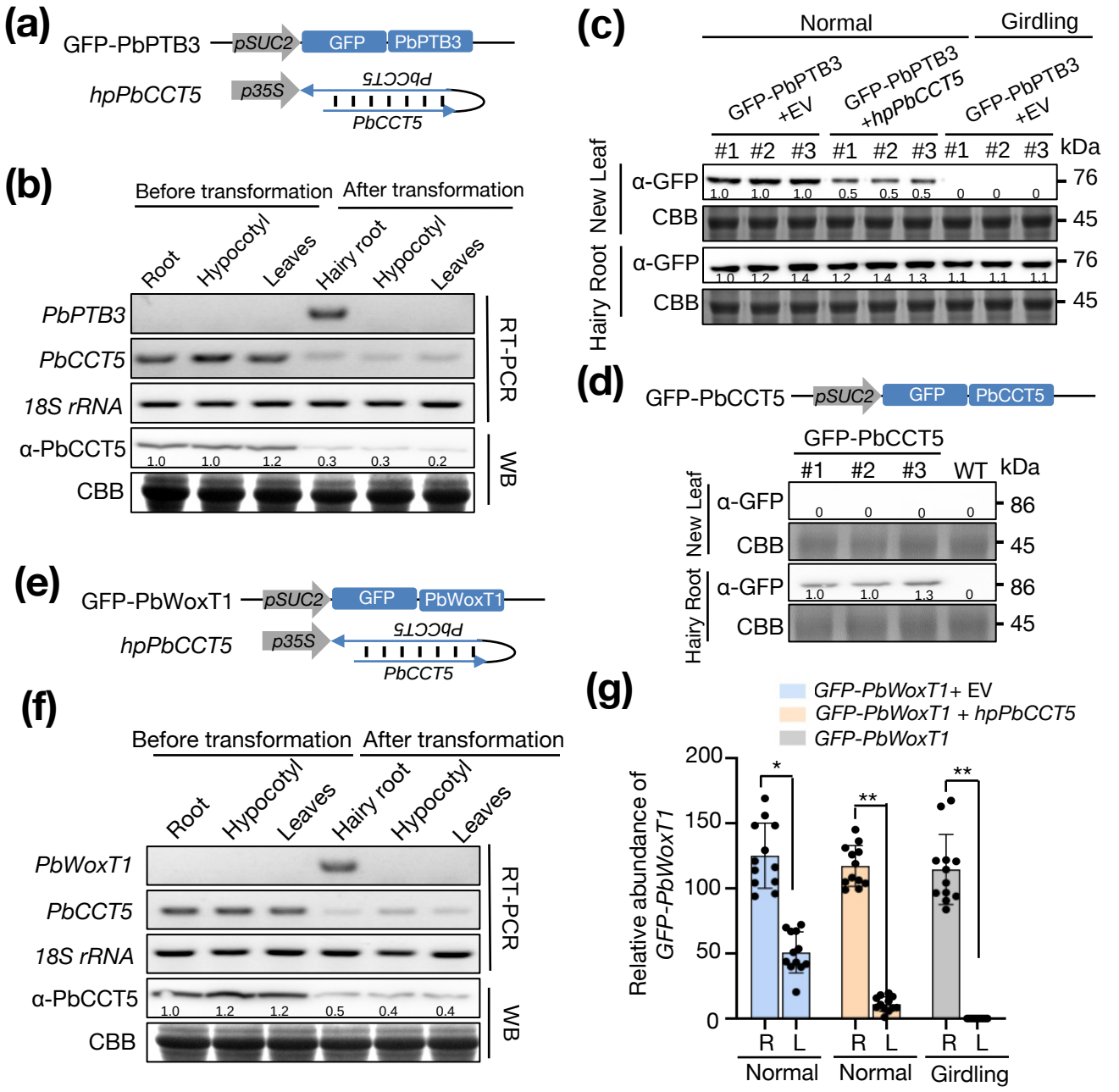

Figure 3

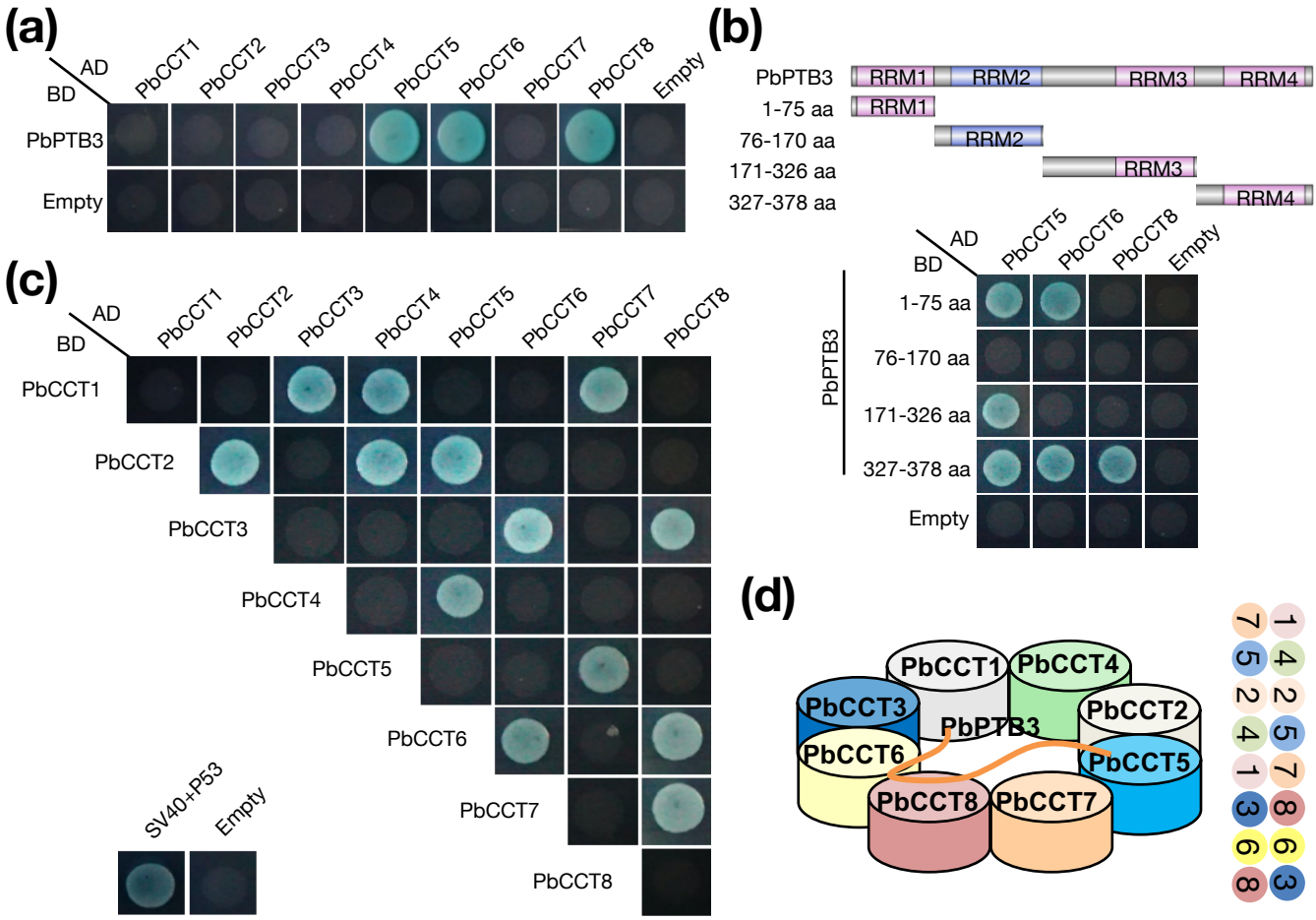

Figure 4

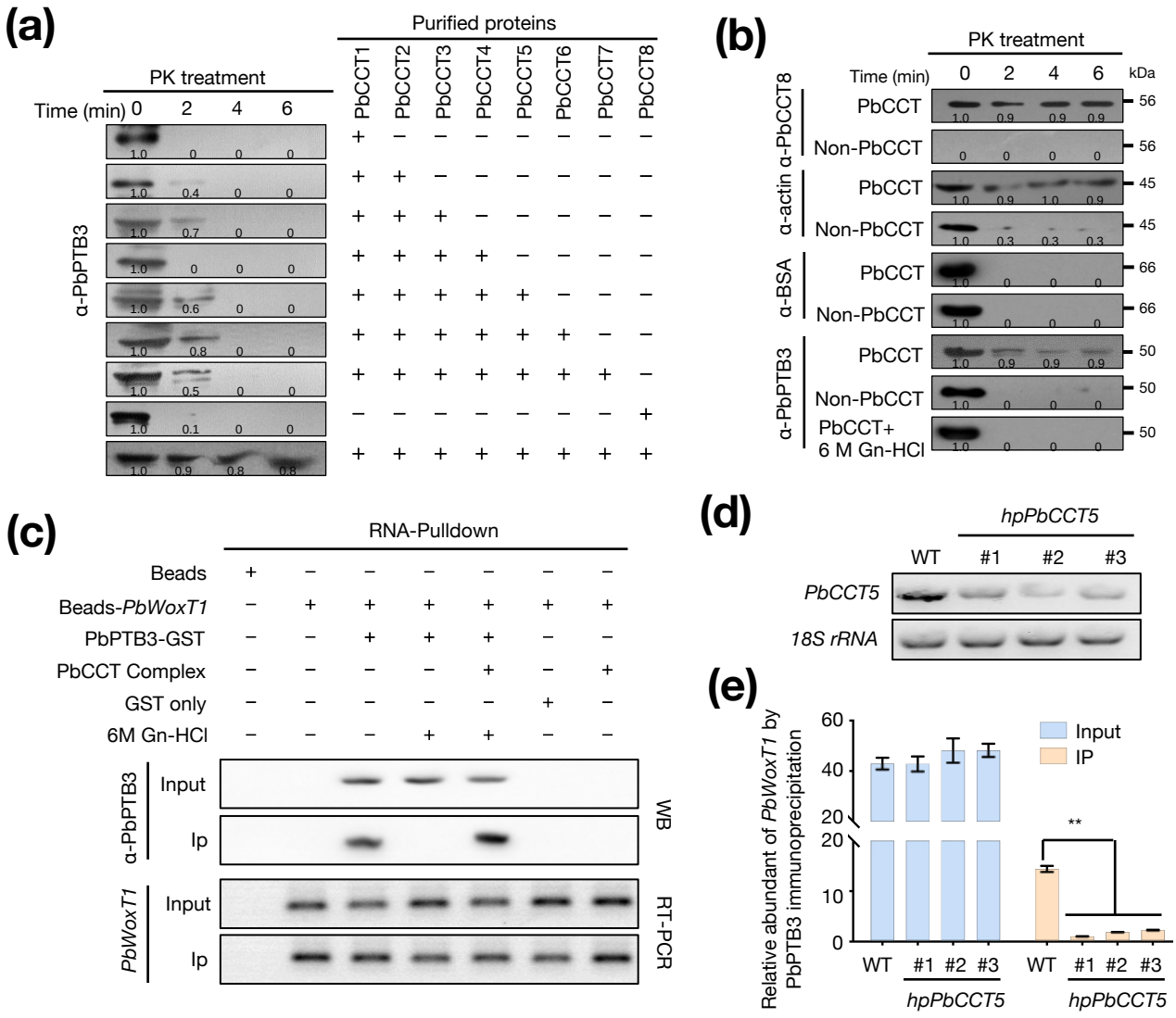

Figure 5